IEEE Access
Multidisciplinary | Rapid Review | Open Access Journal

Received October 8, 2020, accepted October 14, 2020, date of publication October 19, 2020, date of current version October 30, 2020.

Digital Object Identifier 10.1109/ACCESS.2020.3032179

Simulation and Experiment Study on Deformation Characteristics of the Water Hydraulic Flexible Actuator Used for the Underwater Gripper

SONGLIN NIE, XIAOPENG LIU, HUI JI, ZHONGHAI MA, AND FANGLONG YIN
Beijing Key Laboratory of Advanced Manufacturing Technology, Beijing University of Technology, Beijing 100124, China

Corresponding author: Hui Ji (jihui@bjut.edu.cn)

This work was supported in part by the Beijing Natural Science Foundation under Grant 3182003; in part by the National Natural Science Foundation of China under Grant 51905011, Grant 51975010, and Grant 51705008; in part by the Beijing Municipal Science and Technology Project under Grant KM201810005014 and Grant KM201910005033; and in part by the Beijing Postdoctoral Research Foundation under Grant 2020-ZZ-033.

ABSTRACT A water hydraulic flexible gripper with three-fingered structure is developed to deal with the problem of poor adaptability for the existing underwater gripper. This gripper driven by water hydraulics can realize flexible grasping and possess simple structure, high pressure-bearing, strong adaptability and capability of anti-jamming to the water environment and easy to control. In particular, the water hydraulic flexible gripper system is an open system in relation to the underwater environment, with the water source being supplied directly by the underwater environment, eliminating the effects of back pressure generated by the underwater environment in comparison with the closed system of other grippers. It is a good solution to solve the problem of poor adaptability for the existing underwater gripper in underwater environment. The flexible actuator model is established to explore the key parameters influencing the deformation characteristics. The effects of different inlet pressure, knuckle length, wall thickness and material of the inner skeleton and external surface on the deformation characteristics of the flexible actuator are investigated through simulation. It is found that, for the flexible actuator, the wall thickness of the inner skeleton is selected as 1 mm and the inner skeleton length is designed with the first knuckle of 30 mm and the second knuckle of 80 mm. Based on the optimal parameters obtained through simulation, the prototype of flexible actuator and flexible gripper are fabricated. Experiment is performed to test the deformation of the flexible actuator under different inlet pressure. It is found that the experiment results are consistent with the simulation results. Both of the experiment and simulation results exhibit that the total deformation of the flexible actuator is proportional to the inlet pressure. The research will lay foundation for the optimal design of flexible actuator used for the underwater gripper driven by water hydraulics.

INDEX TERMS Deformation characteristics, experimental verification, flexible actuator, numerical simulation, water hydraulic flexible gripper.

I. INTRODUCTION

With the development of economy, especially the exploitation and utilization of the water resources in rivers, lakes and seas, a great number of scientific research underwater, such as biological sampling, environmental monitoring and so on, are gradually dependent on submersible and underwater robots [1]. However, in the past, most of these kinds of works were done by divers, which was expensive and risky. Therefore, as a new technology and method, underwater robot has been gradually applied in underwater scientific research [2]–[4]. At present, the traditional gripper of underwater robot usually adopts rigid actuators driven by motor or hydraulic mechanism. Rigid actuator is normally used to grasp hard materials with good effect, but when grasping flexible or brittle materials, it cannot guarantee that these objects are grasped without being damaged, especially underwater plankton, dangerous substances and various sensitive instruments etc. In addition, the structure of rigid gripper is complex and difficult to control precisely. As the emergence of bionic materials, flexible materials and intelligent materials, flexible actuators made by these materials can adapt to

The associate editor coordinating the review of this manuscript and approving it for publication was Yingxiang Liu.

grasp objects that is flexible or brittle of different shapes and sizes. Flexible gripper with flexible actuators has gradually become a research hotspot [5].

Flexible actuators, a new type of the equipment for robots, have been widely studied by many scholars and institutions. They can be divided into three types by the way of control: dielectric elastomer actuator (DEA), shape memory polymer actuator (SMPA) and pneumatic actuator (PA). Wang *et al*. [6] designed a flexible gripper, which was based on bi-stable DEA. This flexible gripper could achieve good performances in grasping various objects by a simple actuation system. Moreover, when grasping objects, it did not need to provide continuous voltage. The research showed that the soft gripper could grasp objects quickly with very low energy consumption. Xu *et al*. [7] developed a flexible bio-inspired gripper inspired by the grasping process of Venus flytrap. The gripper was driven by DEA, which consisted of a two-leaf functional structure aimed to mimic the leaf closure of the Venus flytrap by controlling the voltage. In addition, the experiment results showed that it took only 0.25 seconds for the gripper to grasp the table tennis ball. All of DEAs can be driven by electrostatic force to meet the needs of artificial muscles [8], [9], however they require a rigid frame to pre-stretch the high elastomer, the preparation process is relatively complex, the reliability of the flexible electrode needs to be further improved, and a higher voltage is needed.

Ge *et al*. [10] developed a flexible gripper with pre-programming function by using a variety of new materials and 4D multi-material printing technology. The structure of shape memory polymer with high resolution and multi material could be created by this technology. Their experimental research showed that the flexible gripper made by SMPAs could grasp a variety of irregular or fragile objects, and could achieve high-precision control. Fang *et al.* [11] mixed ethylene-vinyl acetate and aniline black to provide one candidate material for near-infrared light triggered flexible actuator in aqueous media, and demonstrated the SMPA made by this new material was capable of opening and closing the arms reversibly via periodic variation in irradiation PD successfully. SMPA is suitable for small volume, simple in structure, easy to control, and strong adaptability to the environment [12], [13]. However, it needs to be released through strict temperature changes, which is inefficient. What's more, overheating or excessive strain will easily cause permanent damage to the actuator.

Zhou [14] developed a novel flexible gripper with one passively adaptive palm and three PAs. Each PA comprises two ellipse-profiled pneumatic chambers. The research showed that this flexible gripper could achieve 40 N grasping force in practice, at a very low actuation pressure below 100 KPa by using the ellipse-profile, two-chambered finger, combined with the palm with passive chamber and the surface array pattern. Deimeld and Brock [15] from University of Berlin developed RBO hand, an underactuated flexible gripper based on PA. Due to the poor adaptability of RBO hand to objects and the inability to achieve flexible grasping of more complex objects, they developed RBO hand 2 [16] on the basis of RBO hand by enhancing the learning algorithm to train the flexibility of the gripper. RBO hand 2 had seven PAs, which could achieve four dimensions of grasping, had excellent payload weight ratio, and could grasp objects with a maximum weight of 260 g. At the same time, it had strong flexibility and the ability to resist impact and blunt collision. It could be applied to the working environment containing dust or liquid. Compared with rigid grippers and other flexible grippers, the gripper made up of PA has the characteristics of low pressure-bearing, large deformation and flexible movement [17]–[19]. However, its development is limited by its insufficient rigidity and small grasping force, and cannot adapt to underwater work, especially in deep underwater work.

In addition, many scholars have attempted to combine different types of driving to develop new flexible grippers. Amir Mohammadi Nassab *et al.* [20] designed a three-fingered pneumatic gripper that contains ''programmable'' ligaments that reversibly softens under resistive heating. Moreover, the electrically programmable ligaments was incorporated in the pneumatic actuator had the potential to enhance versatility and reduce dependency on tubing and valves. Xiang *et al.* [21] developed a monolithic flexible-smart gripper with concomitant sensing, actuation, and gripping capabilities. The gripper was consist of a pneumatically actuated visio-tactile (TacTip) sensor and a stretchable EA pad. Completely flexible and safer interactions could be achieved between the actuators and objects. Park *et al.* [22] proposed an electrohydraulic gripper, which was based on electrostatic and hydraulic forces. The gripper could generate a hydraulic force without an external fluid supply source. Researchers investigated the grasp characteristics of the actuator of the gripper and demonstrated the ability of gripper to grasp delicate materials by experiment. Compared with the flexible grippers with a single drive method, the flexible grippers with multiple drive methods have better adaptability, higher gripping efficiency and more accurate control. However, the disadvantages such as low pressure-bearing capacity, complicated control system and small gripping force still exist [19].

It can be seen that these flexible grippers usually possess complex structure, low pressure-bearing, poor adaptability and capability of anti-jamming to the water environment and hard to control. In addition, these flexible gripper systems are closed systems in incompatible to the underwater environment, which are affected by the underwater back pressure environment easily [19], [23], [24]. Therefore, they cannot adapt to complex or special underwater working environment. In this research, a flexible gripper, which can simulate the movement of human hand simply is developed by the bionics principle (as shown in **Figure 1**). The flexible gripper adopts a three-fingered structure, which is composed of three flexible actuators driven by water hydraulics, and can imitate the hand grasping function to the maximum extent. It can not only realize flexible grasping and ensure grasping performance and safety, but also overcome the disadvantages

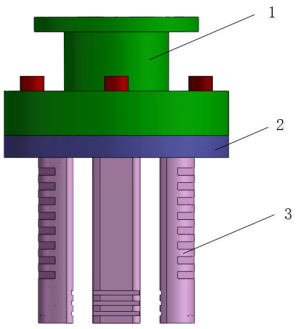

FIGURE 1. Structural of water hydraulic flexible gripper (1-pedestal, 2-connecting tray, 3-flexible actuator).

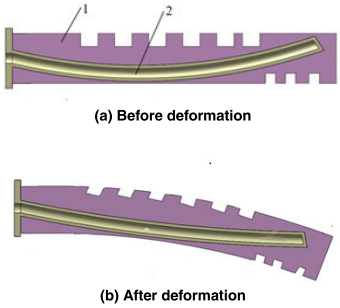

FIGURE 2. Configurations of water hydraulic flexible actuator (1-flexible external surface, 2-inner skeleton).

of existing flexible grippers. The flexible actuator driven by water hydraulics possess simple structure, high pressure-bearing, strong adaptability and capability of anti-jamming to the water environment and easy to control. In particular, the water hydraulic flexible gripper system is an open system in relation to the underwater environment, with the water source being supplied directly by the underwater environment, eliminating the effects of back pressure generated by the underwater environment in comparison with the closed system of other gripper. Therefore, it is well adapted in underwater environment and greatly improve the performance of underwater equipment in the deep underwater working environment. Since three actuators are evenly distributed on the connecting tray, with the same working condition on each actuator, the discussion of the deformation on just one of the actuators will reflect the deformation on the whole gripper. Here the flexible actuator model is established to explore the key parameters influencing the deformation characteristics preliminarily. Simulation comparisons of the effects of different inlet pressure, knuckle length, wall thickness and material of the inner skeleton and external face on the deformation characteristics for the flexible actuator are investigated. Experiment as well as simulation studies will be performed to verify the design and provide a reliable and efficient theoretical basis for the further optimization design of the flexible actuator [25].

II. SETUP OF MODEL

A. WORKING PRINCIPLE OF THE FLEXIBLE ACTUATOR

As a new type of water hydraulic flexible actuator, the flexible actuator consists of corrosion resistant alloy inner skeleton and flexible external surface (as shown in **Figure 2**). Caterpillar's appearance is imitated to design flexible external surface, which has several grooves and protrusions to facilitate the deformation of the flexible actuator and increase external friction to ensure the stability of the grasp. The shape of the inner skeleton is V-shaped along the axis and the section is ellipse. Due to its elliptical section, the inner wall of the inner skeleton is subjected to different forces, and the inner skeleton will gradually straighten from bending when high-pressure water enters into the closed inner skeleton at one end under the control of high-speed switch valve. At the same time, the flexible external surface will bend inward with the deformation of the inner skeleton. What's more, the bending angle of the flexible external surface increases with the increase of pressure. Therefore, the bending deformation of the flexible actuator can be controlled by controlling the pressure of the fluid, and the grasping action of the gripper can be realized.

B. PHYSICAL MODEL

The inner skeleton structure is divided into two knuckles (the first knuckle and the second knuckle), which is shown in **Figure 3 (a)**. In order to achieve the gripping function of the gripper better, it is necessary to optimize the structure of the inner skeleton of the flexible actuator. Further studies will be carried out through simulation to reveal the effect of different length of the first knuckle and second knuckle (l_1 and l_2) on the deformation characteristics of the flexible actuator.

The flexible external surface is designed with several grooves and protrusions to reduce the deformation hindrance by the elastic behavior of the material and increase the deformation of the flexible actuator (as shown in **Figure 2**). Furthermore, this kind of structure can also increase the friction between the external surface of the flexible actuator and the surface of the object to be gripped to ensure a smooth and steady grip when gripping smooth or complex-shaped objects.

C. MATHEMATICAL MODEL

It can be seen from the working principle of the flexible actuator that the inner skeleton plays a very important role in driving the external surface deformation through its own deformation and realizing the gripping action of the flexible actuator. Therefore, the key to understand the deformation characteristics of the flexible actuator is analyzing the deformation characteristics of the inner skeleton. The force and deformation of the inner skeleton within the flexible actuator under the fluid action of pressure P is shown in **Figure 3 (b)**. It is assumed that the inner skeleton material of the flexible actuator is an ideal elasticity with a modulus of elasticity of E, the initial length of inner skeleton without deformed bending deformation is L_0, the average value of inner and outer

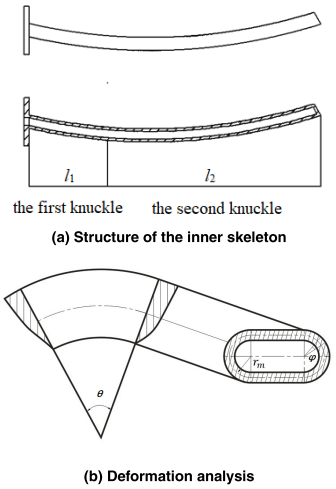

(a) Structure of the inner skeleton

(b) Deformation analysis

FIGURE 3. Schematic of the inner skeleton.

radius of inner skeleton is r_m and the wall thickness of inner skeleton is δ. When the inner skeleton deforms and bends at an angle θ, the polar angle of cross section coordinate system is φ, the axial elongation of the inner skeleton is ΔL, the strain and the stress in the cross section of the inner skeleton is ε and σ respectively. The wall thickness of skeleton is δ' at this time.

The specific solution process is as follows:

$$\Delta L = r_m \theta \sin\varphi \tag{1}$$

Based on the strain formula [26], the strain ε is:

$$\varepsilon = \frac{\Delta L}{L_0} = \frac{r_m \theta \sin\varphi}{L_0} \tag{2}$$

According to Hooke's Law [26], the stress σ in the cross section of the inner skeleton is:

$$\sigma = E\varepsilon = \frac{E r_m \theta \sin\varphi}{L_0} \tag{3}$$

At the same time, the inner skeleton has axial elongation deformation, and its wall thickness becomes δ':

$$\delta' = \frac{\delta L_0}{L_0 + r_m \theta \sin\varphi} \tag{4}$$

III. PHYSICAL CHARACTERIZATION OF MATERIALS

In order to meet the requirements of underwater work, the inner skeleton material of the water hydraulic flexible actuator needs to have high compressive capacity, small inertia, high resilience, high strength and good fatigue resistance. The external surface material of the flexible actuator need to have a certain flexibility, less inertia and high resilience to realize soft and fast grasping. In addition, external surface material should have a certain load-carrying capacity and fit well with the inner skeleton. Moreover, both of the inner skeleton and the flexible external surface materials need to have good corrosion resistances for the flexible actuator needs direct contact with water or seawater.

A. THE INNER SKELETON MATERIALS

After considering the physical properties of materials synthetically, four kinds of materials including high elastic alloy 3J1, 3J21, Titanium alloy and Carbon fiber are selected for comparative study of the inner skeleton material of flexible actuator [27]–[30]. Their specific physical properties are shown in **Table 1**.

TABLE 1. Performance comparison of different inner skeleton materials.

Property (unit)	3J1	3J21	Titanium alloy	Carbon fiber
Density (g/cm^3)	8.0	8.4	4.51	2.0
Tensile strength (MPa)	1372	1323	967	3500
Elastic modulus (GPa)	186	196	128	210
Corrosion resistance	Yes	Yes	Yes	Yes

The elastic modulus of the inner skeleton material of the flexible actuator should not be too small in order to meet the performance requirements of high resilience. At the same time, the specific strength of materials should be great to reduce inertia and achieve precise motion control. Thus, it is more suitable to select titanium alloy as the inner skeleton material of the flexible actuator.

B. THE EXTERNAL SURFACE MATERIALS

Generally, rubber material is a kind of small inertia and high elasticity material, which is widely used in flexible actuator. In this research, three kinds of rubber materials including fluorine rubber, silicone rubber and nitrile rubber are compared and analyzed. Their specific physical properties are listed in **Table 2**. Because of its low strength, poor tear resistance and poor wear resistance, silicone rubber is difficult to meet the application requirements of the flexible external surface materials for the flexible actuator. Fluorine rubber and nitrile rubber have excellent heat resistance, oxidation resistance, corrosion resistance and aging resistance. However, fluorine rubber has poor low temperature performance and unstable physical and chemical properties in underwater cryogenic environment [31]–[35]. Therefore, according to the specific performance requirements of the flexible external surface material of the flexible actuator, nitrile rubber is selected as the flexible external surface material of the flexible actuator.

TABLE 2. Performance comparison of different external surface materials.

Property	Fluorine rubber	Silicone rubber	Nitrile rubber
High temperature resistance	Good	Good	Good
Low temperature resistance	Good	Bad	Normal
Corrosion resistance	Good	Good	Good
Wear resistance	Bad	Normal	Good
Processability	Normal	Normal	Good

IV. SIMULATION ANALYSIS

A. COMPUTATIONAL GRID

A three-dimensional physical model of the flexible actuator is established (as shown in **Figure 2**). Then the mesh is divided through the tetrahedral mesh division function. The mesh model is shown in **Figure 4**.

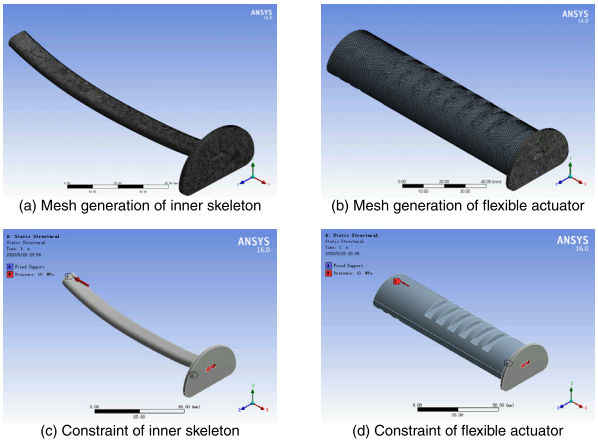

FIGURE 4. Diagram of mesh generation and constraint.

Figure 4(a) shows the mesh model of the inner skeleton. When dividing the mesh, the mesh spacing is 0.5. There are totally 462807 nodes generated, of which the number of Active Elements is 302057. **Figure 4(b)** shows the mesh model of the flexible actuator. When dividing the grid, the mesh spacing is 0.5. There are totally 4505907 nodes generated, of which the number of Active Elements is 3235950. The transition ratio number of the mesh is 0.272, which indicates the quality of the grid preferable.

B. BOUNDARY CONDITIONS AND PARAMETER SETTINGS

As required by actual working conditions, the maximum load on the inner skeleton is 10 MPa during the working process of the flexible actuator. Therefore, the maximum inlet pressure of the flexible actuator during simulation is set to 10 MPa. Furthermore, the pressure applied to the inner skeleton of the flexible actuator is uniform to simulate the action of high-pressure water. At the same time, a full constraint is applied to the intake of the inner skeleton or the intake of the flexible actuator to simulate the axial support of the pedestal and connecting tray to the inner skeleton, as shown in **Figure 4(c, d)**.

C. SIMULATION RESULTS AND ANALYSIS OF THE INNER SKELETON

1) EFFECTS OF DIFFERENT INLET PRESSURE OF THE INNER SKELETON ON THE DEFORMATION CHARACTERISTICS

When all the simulation conditions are identical and only the inlet pressure of inner skeleton is changed, the effects of different inlet pressure on the deformation characteristics of the inner skeleton have been simulated. **Figure 5** shows the total deformation, maximum shear elastic strain and maximum shear stress of the inner skeleton under different inlet pressure. **Figure 6** shows the total deformation of the closed end of the inner skeleton, which is the maximum total deformation of the inner skeleton under different inlet pressure.

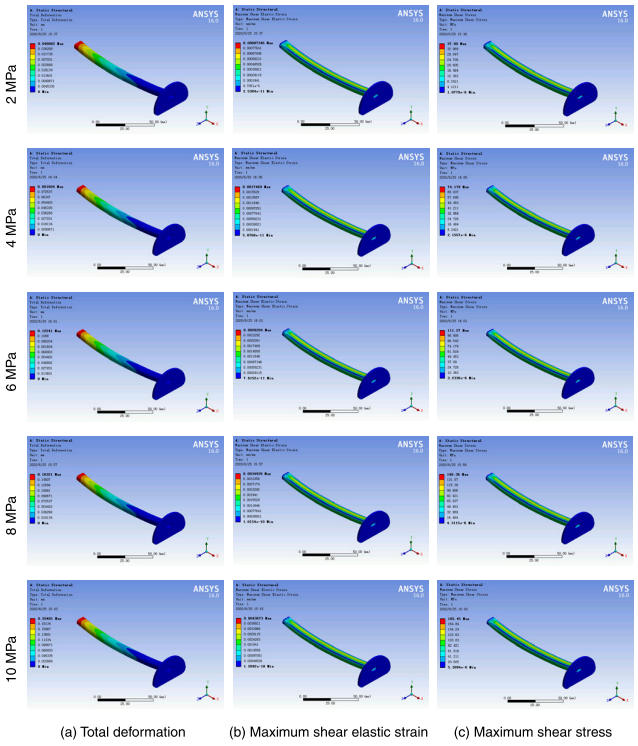

FIGURE 5. Effects of different inlet pressure on the deformation characteristics of the inner skeleton.

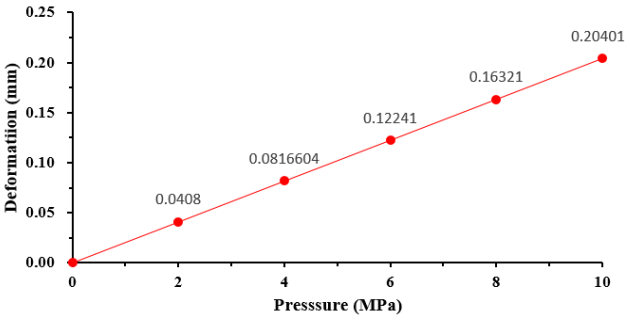

FIGURE 6. Effects of different inlet pressure on the total deformation of the closed end of the inner skeleton.

Figure 5(a) and **Figure 6** show the total deformation of the inner skeleton under different inlet pressure. It indicates that the total deformation of inner skeleton increases gradually with the increasing of inlet pressure. **Figure 5(b)** illustrates the maximum shear elastic strain of inner skeleton under different inlet pressure. It can be found from **Figure 5(b)** that the maximum shear elastic strain of the inner skeleton under different inlet pressure is 4.3673×10^{-3}, which belongs to the safety value within the elastic limit. **Figure 5(c)** demonstrates

the maximum shear elastic stress of the inner skeleton under different inlet pressure. It can be seen from **Figure 5(c)** that the maximum shear elastic stress of the inner skeleton under different inlet pressure is 185.45 MPa, which belongs to the safety value within the elastic limit. It can be obtained from the above results that there is a proportional correlated between the deformation capacity of the inner skeleton and the inlet pressure of the inner skeleton within the elastic range of the material. However, due to the limitations of the actual working equipment and the physical properties of the material, the maximum inlet pressure in this study is set as 10 MPa.

2) EFFECTS OF DIFFERENT MATERIALS OF THE INNER SKELETON ON THE DEFORMATION CHARACTERISTICS

Simulations with different materials of the inner skeleton (including 3J1, 3J21, TC4 and Carbon fiber) have been carried out respectively. When all the simulation conditions are identical and only the material of the inner skeleton is changed, **Figure 7** shows the total deformation, maximum shear elastic strain and maximum shear stress of the inner skeleton with different materials. **Figure 8** shows the total deformation of the closed end of the inner skeleton, which is the maximum total deformation of the inner skeleton with different materials.

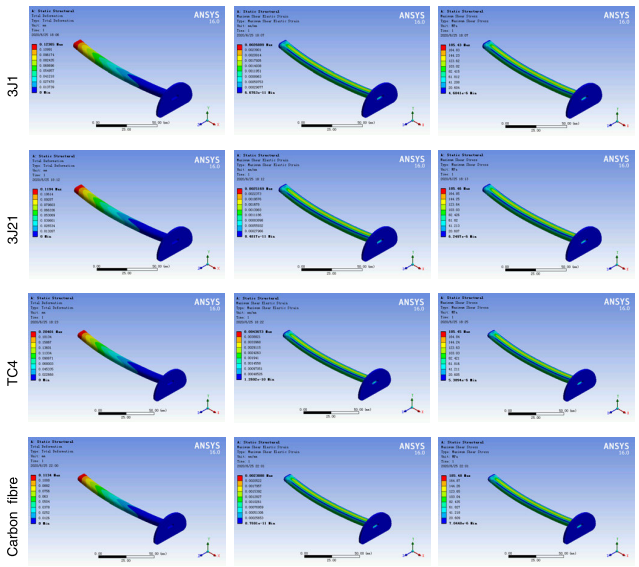

FIGURE 7. Effects of different materials on the deformation characteristics of the inner skeleton.

Figure 7(a) shows the total deformation of inner skeleton with different materials. It can be seen from **Figure 8** that the maximum total deformation of the inner skeleton with 3J1, 3J21, TC4 and Carbon fiber are 0.12365 mm, 0.1194 mm, 0.20401 mm and 0.1134 mm, respectively. **Figure 7(b)**

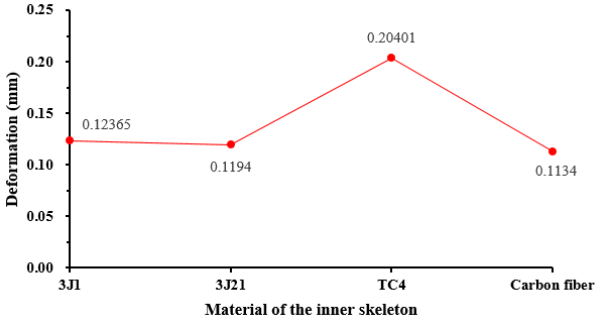

FIGURE 8. Effects of different materials on the total deformation of the closed end of the inner skeleton.

illustrates the maximum shear elastic strain of the inner skeleton with different materials. It can be found from **Figure 7(b)** that the maximum shear elastic strain of the inner skeleton with 3J1, 3J21, TC4 and Carbon fiber are 2.6889×10^{-3}, 2.5169×10^{-3}, 4.3673×10^{-3} and 2.3088×10^{-3}, which belongs to the safety value within the elastic limit, respectively. **Figure 7(c)** demonstrates the maximum shear stress of the inner skeleton with different materials. It can be seen from **Figure 7(c)** that the maximum shear stress of the inner skeleton with 3J1, 3J21, TC4 and Carbon fiber are 185.43 MPa, 185.46 MPa, 185.45 MPa and 185.48 MPa, which belongs to the safety value within the elastic limit, respectively. It can be found from the above results that the deformation ability of the inner skeleton with TC4 is better than the other materials. Therefore, TC4 is a preferential material for the inner skeleton, which can make the inner skeleton has the better ability of deformation.

3) EFFECTS OF DIFFERENT WALL THICKNESS OF THE INNER SKELETON ON THE DEFORMATION CHARACTERISTICS

According to the mathematical model of the inner skeleton and the actual processing conditions, simulations with different wall thickness of inner skeleton, which is set as 1 mm, 1.5 mm, 2 mm, 2.5 mm and 3 mm respectively, have been carried out. When all the simulation conditions are identical and only the wall thickness of inner skeleton is changed, **Figure 9** shows the total deformation, maximum shear elastic strain and maximum shear stress of the inner skeleton under different wall thickness. **Figure 10** shows the total deformation of the closed end of the inner skeleton, which is the maximum total deformation of the inner skeleton under different wall thickness.

Figure 9(a) and**Figure 10** show the total deformation of the inner skeleton under different wall thickness. When the wall thickness of the inner skeleton is set from 1 mm to 3 mm, the total deformation of the inner skeleton decreases gradually with the increasing of wall thickness. **Figure 9(b)** illustrates the maximum shear elastic strain of inner skeleton. It can be seen from **Figure 9(b)** that the maximum shear elastic strain of the inner skeleton is 4.4698×10^{-3},

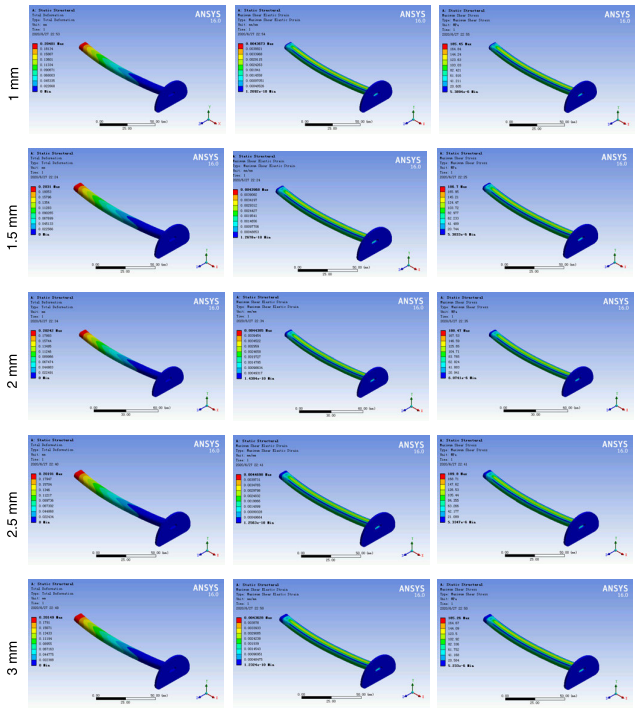

FIGURE 9. Effects of different wall thickness on the deformation characteristics of the inner skeleton.

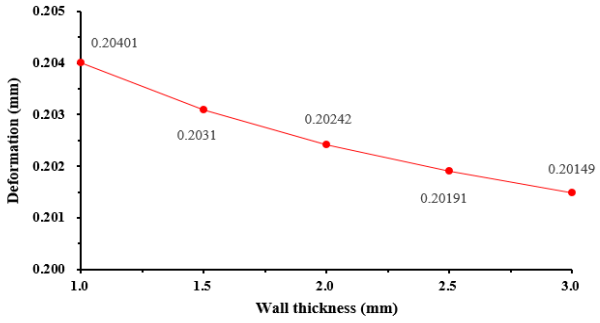

FIGURE 10. Effects of different wall thickness on the total deformation of the closed end of the inner skeleton.

which belongs to the safety value within the elastic limit. **Figure 9(c)** demonstrates the maximum shear elastic stress of inner skeleton. It can be found from **Figure 9(c)** that the maximum shear elastic stress of the inner skeleton is 189.8 MPa, which belongs to the safety value within the elastic limit. It can be concluded from the above results that there is an inversely proportional correlated between the deformation capacity of the inner skeleton and the wall thickness of the inner skeleton within the elastic range of the material. However, due to the limitations of the actual machining conditions and the physical properties of the material, the minimum wall thickness in this study is set as 1 mm.

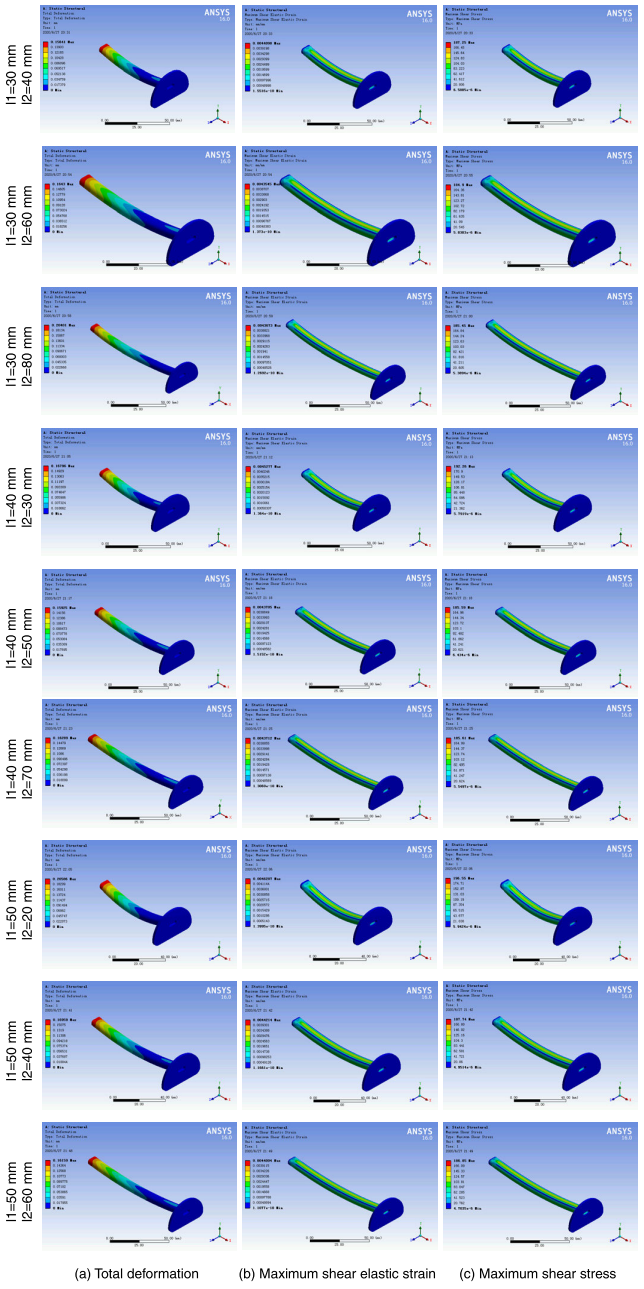

FIGURE 11. Effects of different knuckle length on the deformation characteristics of the inner skeleton.

4) EFFECTS OF DIFFERENT KNUCKLE LENGTH OF THE INNER SKELETON ON THE DEFORMATION CHARACTERISTICS

When all the simulation conditions are identical and only the knuckle length of the inner skeleton is changed, **Figure 11** shows the total deformation, maximum shear elastic strain and maximum shear stress of inner skeleton under different knuckle length. **Figure 12** shows the total deformation of the closed end of the inner skeleton, which is the maximum total deformation of the inner skeleton under different knuckle length. **Figure 11(a)** and **Figure 12** show the total

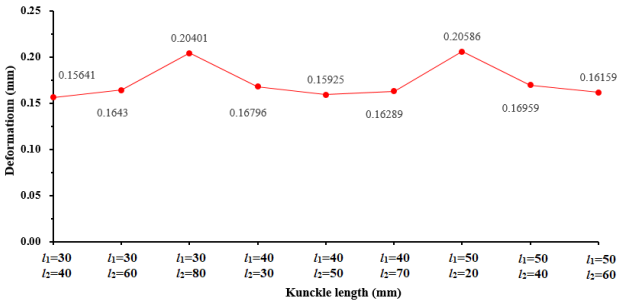

FIGURE 12. Effects of different knuckle length on the total deformation of the closed end of the inner skeleton.

deformation of the inner skeleton under different knuckle length. It can be observed that when the first knuckle is selected as 50 mm and the second knuckle is selected as 20 mm, the total deformation of inner skeleton is bigger than other sizes within the elastic range of the material. The maximum shear elastic strain of the inner skeleton under different knuckle length is demonstrated in **Figure 11(b)**. It can be seen that the maximum shear elastic strain of the inner skeleton under different knuckle length is 4.6287×10^{-3} when the first knuckle is selected as 50 mm and the second knuckle is selected as 20 mm. **Figure 11(c)** illustrates the maximum shear stress of the inner skeleton under different knuckle length. It can be found that when the first knuckle is selected as 50 mm and the second knuckle is selected as 20 mm, the maximum shear stress of inner skeleton is 196.55 MPa, which belongs to the safety value within the elastic limit and occurs where the first knuckle of the inner skeleton is in contact with the gripper's connecting flange.

Figure 11 demonstrates that the ideal inner skeleton length should take into account the effect of the first knuckle length and the second knuckle length on the deformation characteristics. Through simulation analysis, the deformation of the inner skeleton is the largest when the first knuckle is selected as 50 mm and the second knuckle is selected as 20 mm. The deformation of the inner skeleton is the second largest when the first knuckle is selected as 30 mm and the second knuckle is selected as 80 mm. And the largest deformation is only 0.9% larger than the second largest, while the maximum strain and maximum stress of the largest deformation are 6.0% bigger than the second largest deformation. It means that the inner skeleton with the first knuckle of 50 mm and the second knuckle of 20 mm is more prone to fatigue fracture and shorter service life under the same operating condition than the inner skeleton with the first knuckle of 30 mm and the second knuckle of 80 mm. In addition, due to the limitation of overall length of the inner skeleton, the clamping depth of gripper with inner skeleton whose first knuckle of 50 mm and second knuckle of 20 mm is greatly limited when grasping objects with a greater axial length, which will greatly limit the clamping stability and range of application of the gripper. By contrast, the inner skeleton with the first knuckle of 30 mm and second knuckle of 80 mm is more preferable considering deformation, service life, clamping stability and range of grip target.

D. SIMULATION RESULTS AND ANALYSIS OF THE FLEXIBLE ACTUATOR

1) EFFECTS OF DIFFERENT EXTERNAL SURFACE MATERIALS ON THE DEFORMATION CHARACTERISTICS OF THE ACTUATOR

Simulations with different external surface materials (including fluorine rubber, silicone rubber and nitrile rubber) have been carried out respectively. When all the simulation conditions are identical and only the external surface material is changed, **Figure 13** shows the total deformation, maximum shear elastic strain and maximum shear stress of the actuator with different external surface materials. **Figure 14** shows the total deformation of the closed end of the actuator, which is the maximum total deformation of the actuator with different external surface materials.

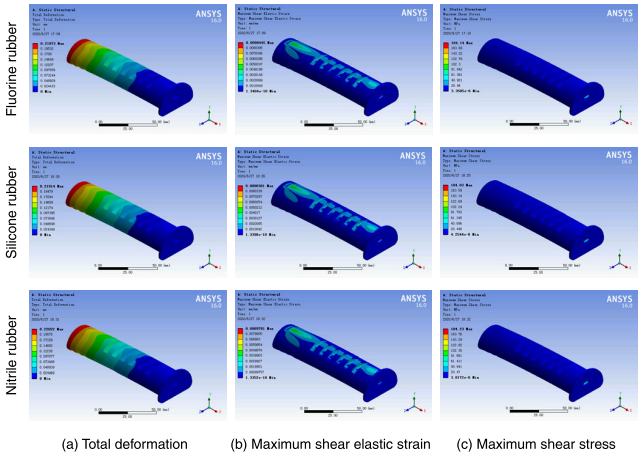

FIGURE 13. Effects of different external surface materials on the deformation characteristics of the actuator.

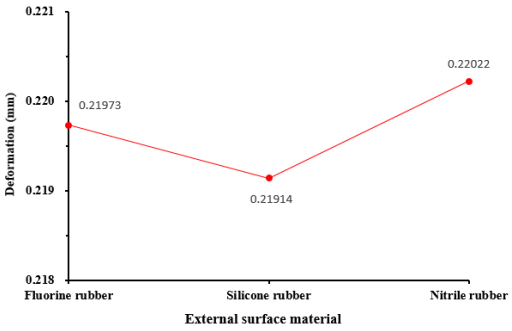

FIGURE 14. Effects of different external surface materials on the total deformation of the closed end of the actuator.

Figure 13(a) and **Figure 14** show the total deformation of the actuator with different external surface materials. It can be seen from **Figure 14** that the maximum total deformation of the actuator with fluorine rubber, silicone rubber and

nitrile rubber are 0.21973 mm, 0.21914 mm and 0.22022 mm, respectively. **Figure 13(b)** illustrates the maximum shear elastic strain of the actuator with different external surface materials. It can be found from **Figure 13(b)** that the maximum shear elastic strain of the actuator with fluorine rubber, silicone rubber and nitrile rubber are 9.0445×10^{-3}, 9.0318×10^{-3} and 8.9781×10^{-3}, which belongs to the safety value within the elastic limit, respectively. **Figure 13(c)** demonstrates the maximum shear stress of actuator with different external surface materials. It can be seen from **Figure 13(c)** that the maximum shear stress of the actuator with fluorine rubber, silicone rubber and nitrile rubber are 184.14 MPa, 184.03 MPa and 184.23 MPa, which belongs to the safety value within the elastic limit, respectively. It can be found from the above results that the three kinds of external surface materials have little influence on the deformation characteristics of the actuator. However, from the view of economy and processing, nitrile rubber is better than the other two materials. Therefore, nitrile rubber is a more suitable material for the external surface.

2) EFFECTS OF DIFFERENT INLET PRESSURE ON THE DEFORMATION CHARACTERISTICS OF THE ACTUATOR

When all the simulation conditions are identical and only the inlet pressure of the actuator is changed, the effects of different inlet pressure on the deformation characteristics of the actuator have been simulated. **Figure 15** shows the total deformation, maximum shear elastic strain and maximum shear stress of the actuator under different inlet pressure.

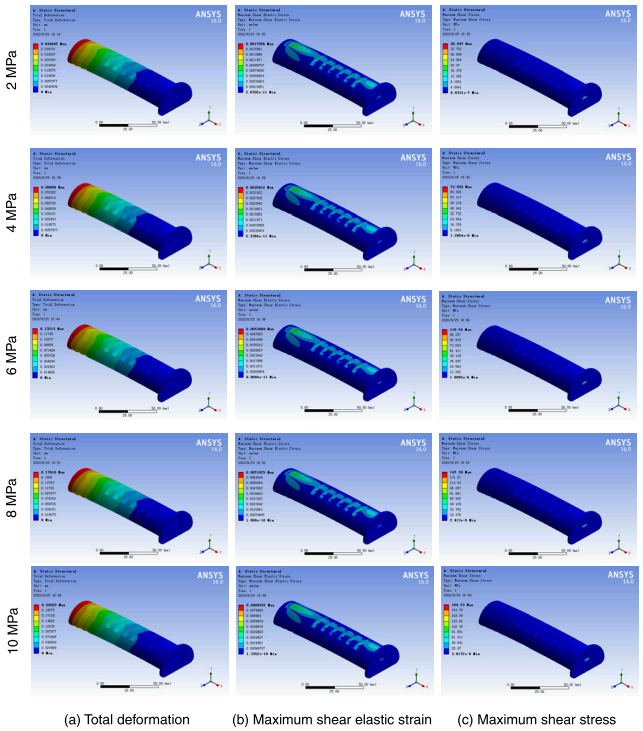

FIGURE 15. Effects of different inlet pressure on the deformation characteristics of the actuator.

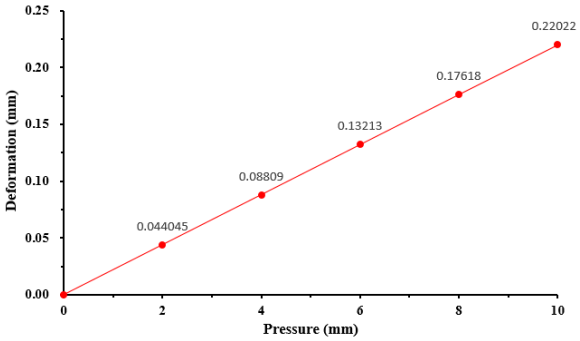

FIGURE 16. Effects of different inlet pressure on the total deformation of the closed end of the actuator.

Figure 16 shows the total deformation of the closed end of the actuator, which is the maximum total deformation of the actuator under different inlet pressure.

Figure 15(a) and **Figure 16** indicate that the total deformation of the actuator increases gradually with the increasing of inlet pressure. **Figure 15(b)** illustrates the maximum shear elastic strain of the actuator under different inlet pressure. It can be found from **Figure 15(b)** that the maximum shear elastic strain of the actuator under different inlet pressure is 8.9781×10^{-3}, which belongs to the safety value within the elastic limit. **Figure 15(c)** demonstrates the maximum shear elastic stress of the actuator under different inlet pressure. It can be seen from **Figure 15(c)** that the maximum shear elastic stress of the actuator under different inlet pressure is 184.23 MPa, which belongs to the safety value within the elastic limit. It occurs where the first knuckle of the inner skeleton is in contact with the gripper's connecting flange. It can be concluded from the above results that there is a proportional correlated between the deformation capacity of the actuator and the inlet pressure of the actuator within the elastic range of the material.

V. EXPERIMENT STUDY

A. EXPERIMENT SYSTEM

Figure 17 shows a schematic diagram of the experiment system. The construction of the system is based on the upgrading of the existing integrated experimental system for water hydraulic components system in the laboratory. The system mainly consists of water hydraulics test bed, flexible gripper control system, flexible gripper and displacement sensor. The displacement sensor is installed in a position near the closed end of the flexible actuator of the flexible gripper, which can test the displacement of the flexible actuator.

As shown in **Figure 17**, a high-pressure water source is supplied to the flexible actuator of the flexible gripper through a water hydraulics test bed. When the pressure shown on the pressure gauge 7 meets the system needs, the high-speed switch valve 8 is closed and the high-speed switch valve 9 is open. The high-pressure water can enter the flexible actuator, which in turn causes it to deform to complete the grasping operation. Meanwhile, the displacement sensor

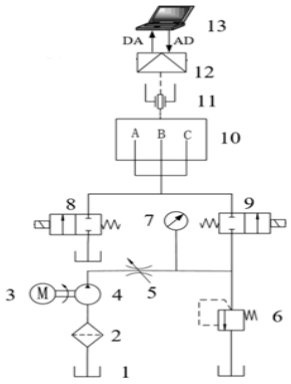

FIGURE 17. Schematic diagram of the experiment system (1-Water tank, 2-filter, 3-Motor, 4-High pressure water pump, 5-Throttle valve, 6-Relief valve, 7-Pressure gauge, 8-High-speed switch valve, 9-High-speed switch valve, 10- Flexible gripper, 11- Displacement sensor, 12- Signal acquisition cabinet, 13-Computer).

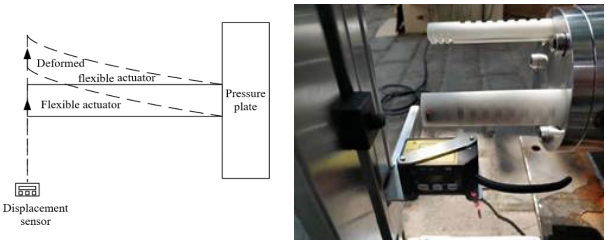

(a) Schematic diagram (b) Physical diagrams

FIGURE 18. Diagram of deformation measurement of flexible actuators.

11 located near the closed end of the flexible actuator detects the deformation produced by the flexible actuator (as shown in **Figure 18(a)**), generates a voltage signal and transmits it to the signal acquisition cabinet 12. The voltage signal collected by the signal acquisition cabinet is imported to the computer and is displayed in real time in the collection interface coded by the LabVIEW software, and the voltage value is converted to the deformation value.

The parameters of the experimental apparatus are as follows: (1) The water hydraulics test bed can provide a pressure range of 0-14 MPa, flowrate of 0-120 L/min. (2) The flexible actuator of the gripper (*i.e.* the optimal structure obtained by simulation): the inner skeleton material is TC4, the wall thickness of the inner skeleton is 1 mm, the inner skeleton length is chosen with 30 mm of the first knuckle and 80 mm of the second knuckle and the external materials is nitrile rubber. (3) The flexible gripper control system: two high-speed switch valves. (4) Displacement sensor: type of MT30, range of 10 mm, repetitive accuracy of 10 μm. (5) High speed acquisition system: modular hardware platform of NI (NI USB-6212 acquisition card) and system design software (LabVIEW).

In this research, 3D printing technology is employed to process flexible actuators. The physical diagrams of the flexible actuator and the flexible gripper are shown in **Figure 18(b)**. The experiment is conducted with the optimal structure of the flexible actuators as the simulation results showed, and test under the same experimental conditions. The inlet pressure of the flexible actuator is considered as variable and is set as 0, 2, 4, 6, 8 and 10 MPa respectively. The diagram of the deformation measurement is shown in **Figure 18**.

B. RESULT AND DISCUSSION

1) EXPERIMENTAL RESULTS OF DIFFERENT INLET PRESSURE

The experiment is performed with optimal flexible actuator structure obtained by simulation to test the deformation of the flexible actuator under different inlet pressure (as shown in **Figure 19**). The experiment results are listed in **Table 3**. As shown in **Table 3** and**Figure 19**, when the inlet pressure is set as 0, 2, 4, 6, 8 and 10 MPa respectively, the minimum and maximum deformation of the flexible actuator are 0 mm and 0.20213 mm, respectively. It can be found from **Figure 19** that the deformation of the actuator increases gradually with the increasing of inlet pressure. There is a proportional correlated between the deformation of the actuator and the inlet pressure of the actuator.

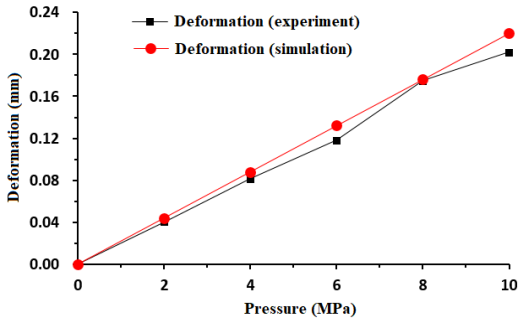

FIGURE 19. Comparisons of simulation and experiment results under different inlet pressure.

TABLE 3. Deformation of the flexible actuator under different inlet pressure.

Number	Inlet pressure (MPa)	Deformation (mm)
1	0	0
2	2	0.04037
3	4	0.08145
4	6	0.11830
5	8	0.17490
6	10	0.20213

2) COMPARISONS OF SIMULATION AND EXPERIMENT RESULTS

To validate the effects of different inlet pressure on the deformation of the flexible actuator, the comparisons between simulation and experiment results are conducted. **Figure 19** shows the deformation of the simulation and experiment results under different inlet pressure for the flexible actuator. It can be observed that the experiment value is slightly smaller

than the simulation value. This is because the flexible actuator processing method used in this experiment is 3D printing, which will have an effect on the elasticity and plasticity of the material [36]–[37]. However, the trends of the simulation and experiment are similar, and with the increase of inlet pressure, the deformation of the flexible actuator is also increasing gradually. This exhibits that the simulation model built in this research is essentially correct, and the simulation results are consistent with the experiment results.

Through the simulation and experimental study, it is proved that the deformation of flexible actuator is driven by the inner skeleton. Therefore, the key to the development of flexible actuator is to study the deformation characteristics of inner skeleton. In this research, the flexible actuator with TC4 as the inner skeleton material is easy to achieve precise control of deformation, however, its deformation is not large. This is attributed to the fact that the physical and chemical properties of TC4 are limited and it is unable to have good elasticity and plasticity with high strength at the same time, which means the inner skeleton cannot achieve large deformation while withstanding high pressure. As a result, the gripper with these flexible actuators can only grasp a limited number of objects and has a limited range of application. This problem would be solved in the future by screening new inner skeleton materials, which will have good elasticity and plasticity with high strength at the same time and can effectively increase the deformation of the flexible actuator and expand the application scope of the flexible gripper. In addition, the cross-section of the inner skeleton is elliptical, which makes the inner wall subjected to different forces to deform. In the further study, the structure of the inner skeleton will be optimized to increase the force differential between the inner walls of the inner skeleton or reduce the deformation resistance of the inner skeleton, which will also help increase the deformation of the flexible actuator.

VI. CONCLUSION

In this research, a novel flexible underwater gripper driven by water hydraulics is developed, which can simply imitate the movement of human hand. The flexible gripper adopts a three-fingered structure, which is composed of three water-hydraulically driven flexible actuators. The flexible actuator model is established to explore the key parameters influencing the deformation characteristics. Simulation comparisons of the effects of different inlet pressure, knuckle length, wall thickness and material of the inner skeleton and external on the deformation characteristics for flexible actuator are performed. Experiment is performed to test the deformation of the flexible actuator under different inlet pressure. Both of the experiment and simulation results indicate that the flexible actuator can realize deformation, which can help the flexible underwater gripper achieve grasping function.

The following conclusions can be drawn from this research: (1) The total deformation of the flexible actuator is proportional to the inlet pressure, and is inversely proportional to the wall thickness of inner skeleton. Therefore, the higher inlet pressure and the thinner wall thickness of inner skeleton are more conducive to the larger deformation of the flexible actuator within the elastic range of the material. When designing flexible actuators in the future, the pressure-bearing capacity of the inner skeleton should be improved and the wall thickness of the inner skeleton should be reduced as much as possible to produce large deformations, so as to expand the application range of the gripper. (2) According to the conditions of actual working equipment, the maximum inlet pressure is set as 10 MPa. When the wall thickness of the inner skeleton is selected as 1 mm, the deformation of the flexible actuator can get the largest. (3) The inner skeleton with the first knuckle of 30 mm and second knuckle of 80 mm is more preferable considering deformation, service life, clamping stability and range of grip target. (4) TC4 is a more preferential material for the inner skeleton and nitrile rubber is a more preferential material for the external surface when taking into account of the deformation, economy and processability.

NOMENCLATURE

- L_0 —— Initial length of inner skeleton (mm);
- ΔL —— Deformation of inner skeleton (mm);
- l_1 —— Length of the first knuckle of inner skeleton (mm);
- l_2 —— Length of the second knuckle of inner skeleton (mm);
- P —— Inlet pressure (MPa);
- δ —— Wall thickness of inner skeleton (mm);
- δ' —— Wall thickness of inner skeleton after deformation (mm);
- θ —— Deformation angle of inner skeleton (Degree);
- r_m —— Middle value of inner and outer radius of inner skeleton (mm);
- ε —— Strain in the cross section of the inner skeleton;
- σ —— Stress in the cross section of the inner skeleton (MPa);
- E —— Elastic modulus of inner skeleton material (MPa).

REFERENCES

[1] X. Xiang, Z. Niu, L. Lapierre, and M. Zuo, "Hybrid underwater robotic vehicles: The state-of-the-art and future trends," *HKIE Trans.*, vol. 22, no. 2, pp. 103–116, Apr. 2015.

[2] L. C. Lund-Hansen, T. Juul, T. D. Eskildsen, I. Hawes, B. Sorrell, C. Melvad, and K. Hancke, "A low-cost remotely operated vehicle (ROV) with an optical positioning system for under-ice measurements and sampling," *Cold Regions Sci. Technol.*, vol. 151, pp. 148–155, Jul. 2018.

[3] P. Ridao, M. Carreras, D. Ribas, P. J. Sanz, and G. Oliver, "Intervention AUVs: The next challenge," *Annu. Rev. Control*, vol. 40, pp. 227–241, Jan. 2015.

[4] P. Yu, L. Wang, J. Jin, Z. Ye, and D. Chen, "A novel piezoelectric actuated underwater robotic finger," *Smart Mater. Struct.*, vol. 28, no. 10, Oct. 2019, Art. no. 105047.

[5] S. Sivčev, J. Coleman, E. Omerdić, G. Dooly, and D. Toal, "Underwater manipulators: A review," *Ocean Eng.*, vol. 163, pp. 431–450, Sep. 2018.

[6] Y. Wang, U. Gupta, N. Parulekar, and J. Zhu, "A soft gripper of fast speed and low energy consumption," *Sci. China Technol. Sci.*, vol. 62, no. 1, pp. 31–38, Jan. 2019.
[7] L. Xu and G. Gu, "Bioinspired Venus flytrap: A dielectric elastomer actuated soft gripper," in *Proc. 24th Int. Conf. Mechatronics Mach. Vis. Pract. (M2VIP)*, Nov. 2017, pp. 1–3.
[8] U. Gupta, L. Qin, Y. Wang, H. Godaba, and J. Zhu, "Soft robots based on dielectric elastomer actuators: A review," *Smart Mater. Struct.*, vol. 28, no. 10, Oct. 2019, Art. no. 103002.
[9] T. K. Das, B. Shirinzadeh, M. Ghafarian, and A. Al-Jodah, "Design, analysis, and experimental investigation of a single-stage and low parasitic motion piezoelectric actuated microgripper," *Smart Mater. Struct.*, vol. 29, no. 4, Apr. 2020, Art. no. 045028.
[10] Q. Ge, A. H. Sakhaei, H. Lee, C. K. Dunn, N. X. Fang, and M. L. Dunn, "Multimaterial 4D printing with tailorable shape memory polymers," *Sci. Rep.*, vol. 6, no. 1, p. 31110, Nov. 2016.
[11] L. Fang, T. Fang X. Liu, S. Chen, C. Lu, and Z. Xu, "Near-infrared light triggered soft actuators in aqueous media prepared from shape-memory polymer composites," *Macromol. Mater. Eng.*, vol. 301, no. 9, pp. 1111–1120, 2016.
[12] A. Nespoli, S. Besseghini, S. Pittaccio, E. Villa, and S. Viscuso, "The high potential of shape memory alloys in developing miniature mechanical devices: A review on shape memory alloy mini-actuators," *Sens. Actuators A, Phys.*, vol. 158, no. 1, pp. 149–160, Mar. 2010.
[13] C. Kim, G. Kim, Y. Lee, G. Lee, S. Han, D. Kang, S. H. Koo, and J.-S. Koh, "Shape memory alloy actuator-embedded smart clothes for ankle assistance," *Smart Mater. Struct.*, vol. 29, no. 5, May 2020, Art. no. 055003.
[14] J. Zhou, S. Chen, and Z. Wang, "A soft-robotic gripper with enhanced object adaptation and grasping reliability," *IEEE Robot. Autom. Lett.*, vol. 2, no. 4, pp. 2287–2293, Oct. 2017.
[15] R. Deimel and O. Brock, "A compliant hand based on a novel pneumatic actuator," in *Proc. IEEE Int. Conf. Robot. Autom.*, May 2013, pp. 2047–2053.
[16] R. Deimel and O. Brock, "A novel type of compliant and underactuated robotic hand for dexterous grasping," *Int. J. Robot. Res.*, vol. 35, nos. 1–3, pp. 161–185, Jan. 2016.
[17] T. Rehman, M. Nafea, A. A. Faudzi, T. Saleh, and M. S. M. Ali, "PDMS-based dual-channel pneumatic micro-actuator," *Smart Mater. Struct.*, vol. 28, no. 11, Nov. 2019, Art. no. 115044.
[18] M. D. Volder and D. Reynaerts, "Pneumatic and hydraulic microactuators: A review," *J. Micromech. Microeng.*, vol. 20, no. 4, 2010, Art. no. 043001.
[19] J. Shintake, V. Cacucciolo, D. Floreano, and H. Shea, "Soft robotic grippers," *Adv. Mater.*, vol. 30, no. 29, Jul. 2018, Art. no. 1707035.
[20] A. M. Nasab, A. Sabzehzar, M. Tatari, C. Majidi, and W. Shan, "A soft gripper with rigidity tunable elastomer strips as ligaments," *Soft Robot.*, vol. 4, no. 4, pp. 411–420, Dec. 2017.
[21] C. Xiang, J. Guo, and J. Rossiter, "Soft-smart robotic end effectors with sensing, actuation, and gripping capabilities," *Smart Mater. Struct.*, vol. 28, no. 5, May 2019, Art. no. 055034.
[22] T. Park, K. Kim, S.-R. Oh, and Y. Cha, "Electrohydraulic actuator for a soft gripper," *Soft Robot.*, vol. 7, no. 1, pp. 68–75, Feb. 2020.
[23] Z. Zhang, X. Li, X. Yu, H. Chai, Y. Li, H. Wu, and S. Jiang, "Magnetic actuation bionic robotic gripper with bistable morphing structure," *Compos. Struct.*, vol. 229, Dec. 2019, Art. no. 111422.
[24] W.-B. Li, W.-M. Zhang, H.-X. Zou, Z.-K. Peng, and G. Meng, "Multisegment annular dielectric elastomer actuators for soft robots," *Smart Mater. Struct.*, vol. 27, no. 11, Nov. 2018, Art. no. 115024.
[25] Y. H. Huang, J. L. Yu, Z. H. Liu, B. Hu, Z. F. Guan, and H. M. Liu, "Dynamic and static characteristics analysis of stacking manipulator based on ANSYS workbench," *Mech. Eng.*, no. 12, pp. 69–70, Dec. 2016.
[26] Z. L. Xu, *Applied Elasticity*. Beijing, China: Higher Education Press, 1992.
[27] J. B. Zhou, "Chemical polishing process of 3J1 elastic alloy," *Mater. Protection*, no. 7, pp. 31–32, Jul. 1998.
[28] X. O. Jin, S. Y. He, and W. B. Xue, "Fatigue behavior of 3J21 alloy at different aged states," *J. Mater. Eng.*, vol. 25, no. 6, pp. 26–27, 2007.
[29] Y. Song, F. S. Zhang, T. Huang, and K. X. Song, "Study on thermal deformation behavior of TC4-ELI titanium alloy," in *Proc. IOP Conf. Ser., Mater. Sci. Eng.*, vol. 359, Nov. 2017, pp. 1–6.
[30] B. Ravi and M. S. Gupta, "Design and development of automotive carbon fiber bracket," in *Proc. IOP Conf. Ser., Mater. Sci. Eng.*, vol. 455, Jul. 2018, pp. 1–5.
[31] W. L. Wu and H. H. Feng, "Study on short basalt fiber reinforced fluorine rubber composites," *Adv. Mater. Res.*, vol. 1052, pp. 258–261, Oct. 2014.
[32] L. Yan, K. Kou, T. Ji, G. Liang, and E. Ha, "Application of a new modified epoxy adhesive for bonding fluorine rubber to metal," *J. Adhes. Sci. Technol.*, vol. 21, no. 15, pp. 1483–1496, Jan. 2007.
[33] M. Kozako, M. Higashikoji, T. Tominaga, M. Hikita, G. Ueta, S. Okabe, and T. Tanaka, "Fabrication of silicone rubber nanocomposites and quantitative evaluation of dispersion state of nanofillers," *IEEE Trans. Dielectr. Electr. Insul.*, vol. 19, no. 5, pp. 1760–1767, Oct. 2012.
[34] L. Bailly, M. Toungara, L. Orgéas, E. Bertrand, V. Deplano, and C. Geindreau, "In-plane mechanics of soft architectured fibre-reinforced silicone rubber membranes," *J. Mech. Behav. Biomed. Mater.*, vol. 40, pp. 339–353, Dec. 2014.
[35] S. Z. Xie, *Handbook of Rubber Industry*. Beijing, China: Chemical Industry Press, 1989.
[36] P. Barriobero-Vila, J. Gussone, A. Stark, N. Schell, J. Haubrich, and G. Requena, "Peritectic titanium alloys for 3D printing," *Nature Commun.*, vol. 9, no. 1, p. 3426, Dec. 2018.
[37] Y. J. Liu, S. J. Li, H. L. Wang, W. T. Hou, Y. L. Hao, R. Yang, T. B. Sercombe, and L. C. Zhang, "Microstructure, defects and mechanical behavior of beta-type titanium porous structures manufactured by electron beam melting and selective laser melting," *Acta Mater.*, vol. 113, pp. 56–67, Jul. 2016.

SONGLIN NIE was born in Hubei, China, in 1967. He received the Ph.D. degree in mechanical engineering from the Huazhong University of Science and Technology (HUST), China, in 2002.

From 2002 to 2009, he has been an Associate Professor from 2002 to 2006 and a Professor from 2006 to 2009 with the Department of Mechanical Engineering, Huazhong University of Science and Technology, respectively. From 2004 to 2005, he worked as a Visiting Professor with the Faculty of Engineering, University of Regina, Regina, SK, Canada. Since 2009, he has been a Professor with the College of Mechanical Engineering and Applied Electronics Technology, Beijing University of Technology, China. He is the author of one book, more than 150 articles, and more than 80 inventions. His current research interests include the component development, dynamics analyses and simulation of water hydraulics and robots, contamination modeling and assessment, optimization design and control, and of fluid power systems under uncertainty.

Dr. Nie was a recipient of the New Century Excellent Talents Program of the Ministry of Education (NCET-07-0330), in 2007, a distinguished Professor of Beijing (PHR-IHLB 20090203), in 2009, and a Greatwall Scholar of Beijing (CIT&TCD 20130316), in 2012. He is a Senior Member of the China Society of Mechanical Engineering and a Fellow of Fluid Transmission and Control Branch, China.

XIAOPENG LIU was born in Henan, China, in 1994. He received the B.S. degree in mechanical engineering from Inner Mongolia Agricultural University, China, in 2018. He is currently pursuing the master's degree in mechanical engineering. He is also a Research Assistant with the College of Mechanical Engineering and Applied Electronics Technology, Beijing University of Technology, Beijing, China.

HUI JI was born in Hebei, China, in 1987. She received the M.S. and Ph.D. degrees in mechanical engineering from the Beijing University of Technology, Beijing, China, in 2013 and 2017, respectively.

From 2017 to 2019, she was a Postdoctoral Fellow with the Beijing University of Technology, where she has been an Assistant Professor with the College of Mechanical Engineering and Applied Electronics Technology, since 2018. Her current research interests include contamination control of fluid power systems, dynamics analyses and simulation of water hydraulics and robots, and pollution control technology based on SED and hydrodynamic cavitation. She is a Senior Member of the China Society of Mechanical Engineering.

ZHONGHAI MA was born in Gansu, China, in 1993. He received the B.S. and Ph.D. degrees in mechatronics engineering from Beihang University, Beijing, China, in 2015 and 2019, respectively. Since 2019, he has been a Postdoctoral Fellow with the Beijing University of Technology, Beijing, where he has also been an Assistant Professor, since 2020. His research interests include accelerated life test theory, performance degradation modeling and life assessment technology of hydraulic components, prognostic, and health management for mechatronic systems.

FANGLONG YIN was born in Anhui, China, in 1989. He received the Ph.D. degree in mechanical engineering from the Beijing University of Technology, Beijing, China, in 2015.

From 2015 to 2017, he was a Postdoctoral Fellow with the Beijing University of Technology, where he has been an Associate Professor with the College of Mechanical Engineering and Applied Electronics Technology, since 2019. His current research interests include water hydraulic transmission technology, energy recovery technology for seawater reverse osmosis, and marine electro-mechanical equipment. He is a Senior Member of the China Society of Mechanical Engineering.